Electronic supplementary materials

for https://doi.org/10.1631/jzus.A2200528

Fractal analysis of small-micro pores and estimation of permeability of loess using mercury intrusion porosimetry

Tuo LU[1,2], Yaming TANG[3]✉, Yongbo TIE[4], Bo HONG[3], Wei FENG[3]

[1]*Chinese Academy of Geological Sciences, Beijing 100037, China*

[2]*China University of Geosciences, Beijing 100083, China*

[3]*Xi'an Center of China Geological Survey, Xi'an 710054, China*

[4]*Chengdu Center of China Geological Survey, Chengdu 610081, China*

✉ Yaming TANG, tangyaming@mail.cgs.gov.cn

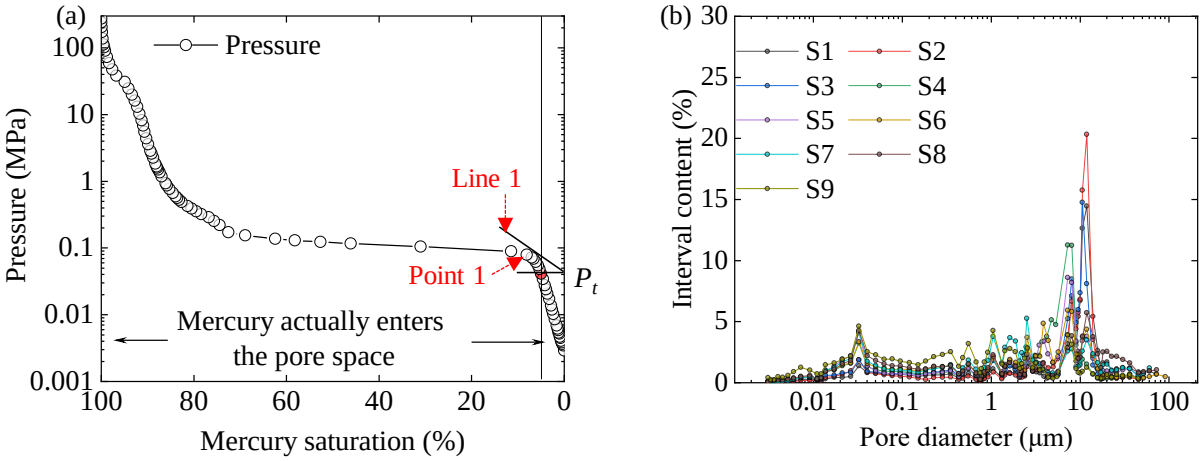

Fig. S1 The determination of pore size range and pore diameter distribution. (a) The determination of the largest diameter: Point 1 is the first turning point after the end of the plateau on the Pressure-Mercury curve, and Line 1 is the tangent line to the point 1. P_t is the intersection of line 1 and Pressure-axis. (b) Pore diameter distribution

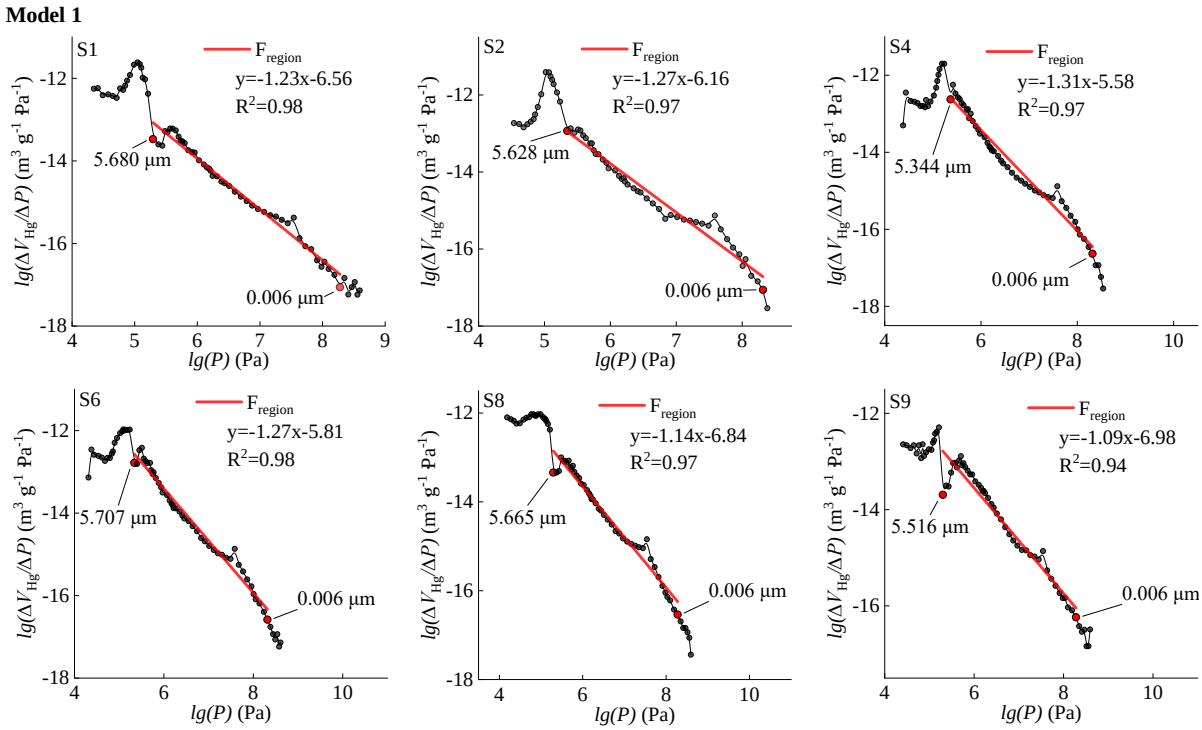

Fig. S2 Plots of lg(P) vs. lg($\Delta V_{Hg}/\Delta P$) for the samples (Model 1). The fractal dimensions are shown in Table 4

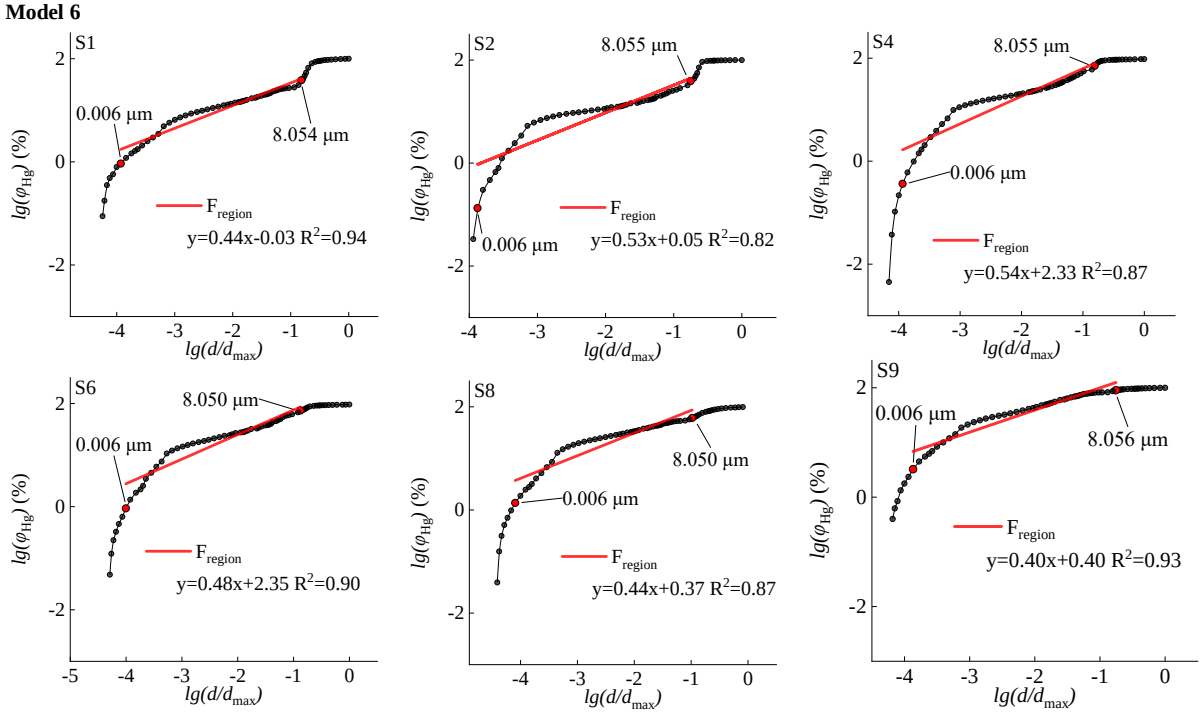

Fig. S3 Plots of lg(d/d_{max}) vs. lg(φ_{Hg}) for samples (Model 6). The fractal dimensions are shown in Table 4

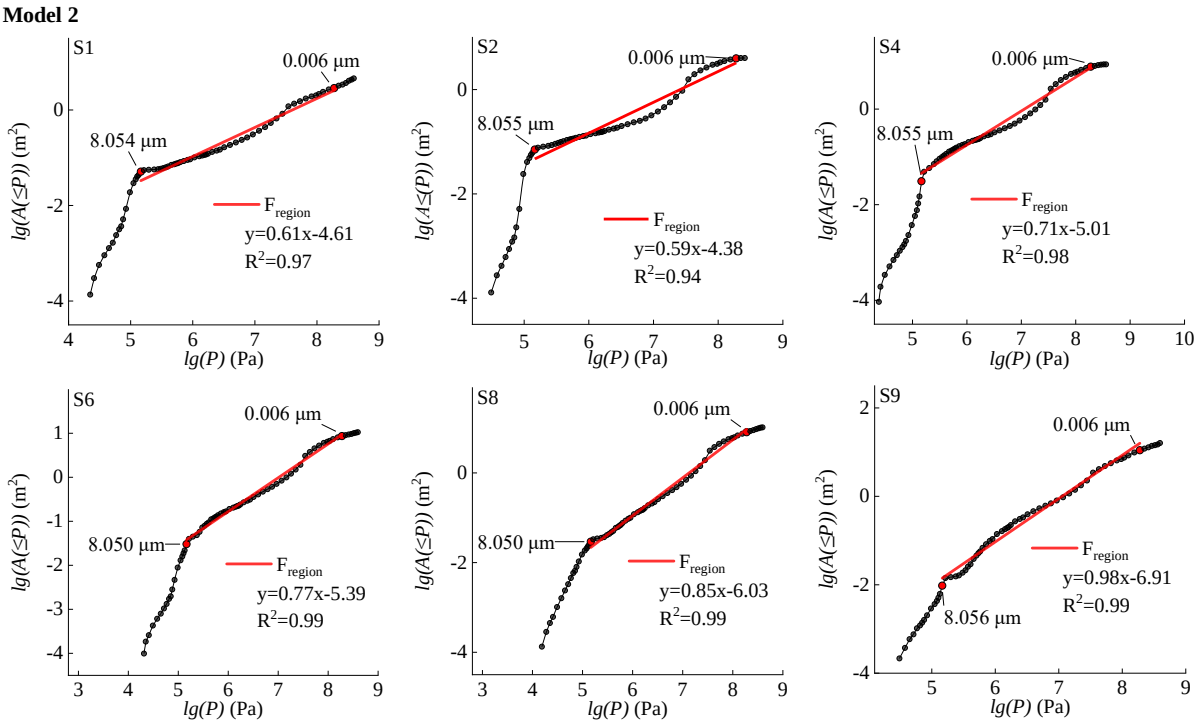

Fig. S4 Plots of lg(P) vs. lg(A(≤P)) for the samples (Model 2). The fractal dimensions are shown in Table 4

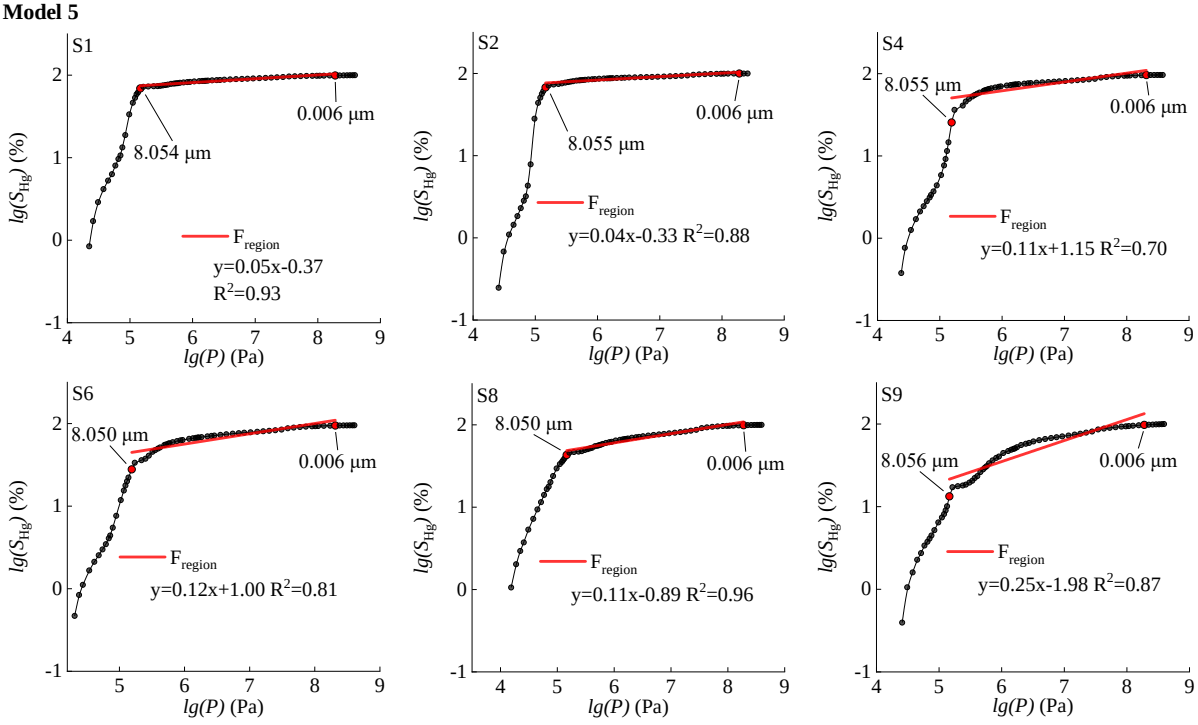

Fig. S5 Plots of lg(P) vs. lg(S_{Hg}) for the samples (Model 5). The fractal dimensions are shown in Table 4

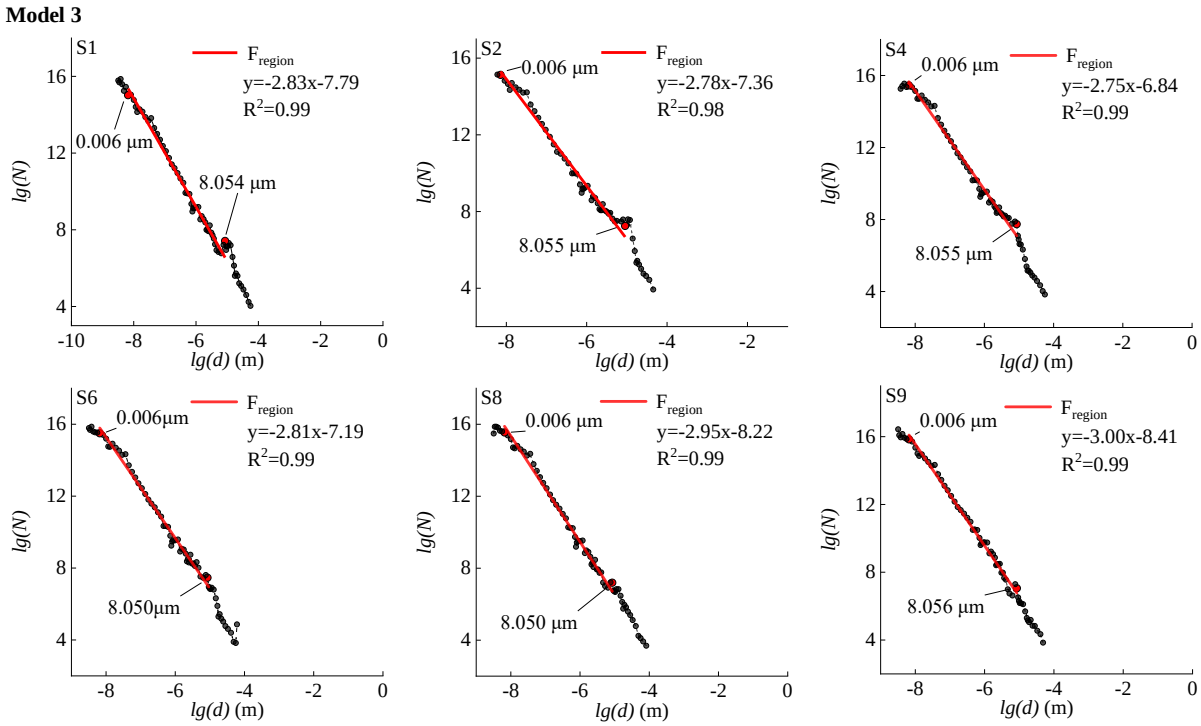

Fig. S6 Plots of lg(d) vs. lg(N) for the samples (Model 3). The fractal dimensions are shown in Table 4

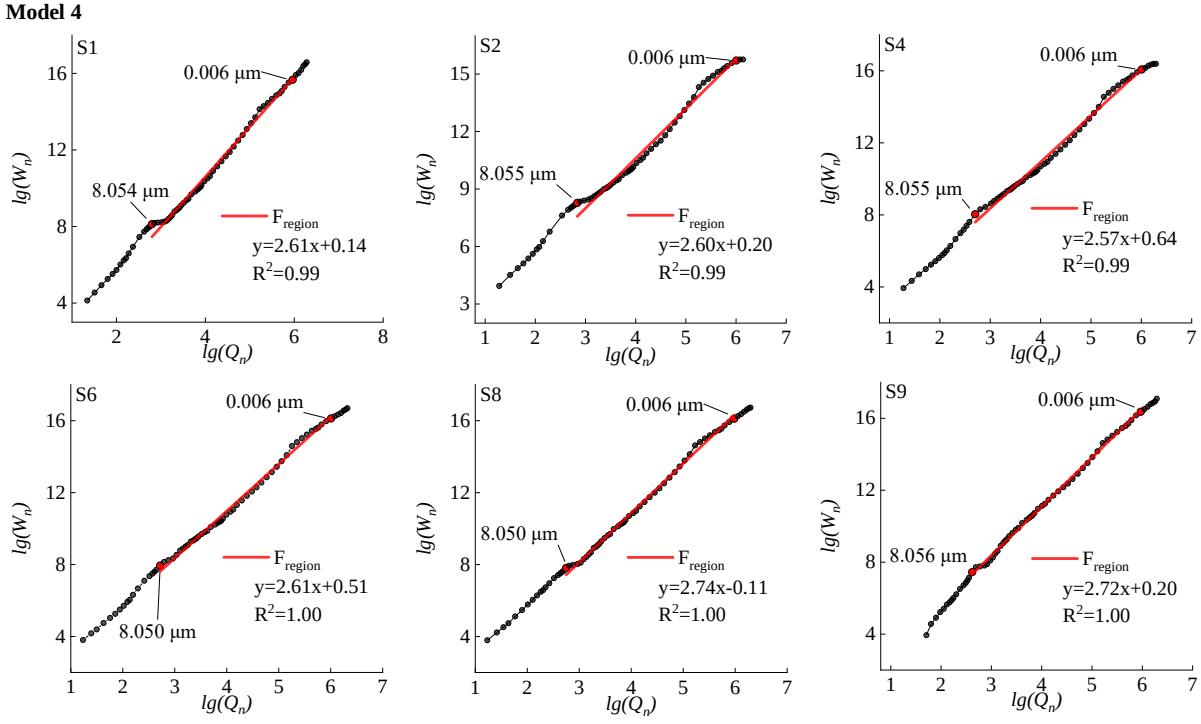

Fig. S7 Plots of lg(Qn) vs. lg(Wn) for the samples (Model 4). The fractal dimensions are shown in Table 4